Effects of Protic and Aprotic Solvents in Mesoporous Silica: Tuning the UV−Vis Emission Properties by Means of Surface Activation

ARTICLE *in* THE JOURNAL OF PHYSICAL CHEMISTRY C · OCTOBER 2014

Impact Factor: 4.77 · DOI: 10.1021/jp508857t

5 AUTHORS, INCLUDING:

Carlo Maria Carbonaro
Università degli studi di Cagliari
80 PUBLICATIONS **782** CITATIONS
SEE PROFILE

P.C. Ricci
Università degli studi di Cagliari
104 PUBLICATIONS **751** CITATIONS
SEE PROFILE

Daniele Chiriu
Università degli studi di Cagliari
29 PUBLICATIONS **107** CITATIONS
SEE PROFILE

THE JOURNAL OF PHYSICAL CHEMISTRY C

Article

pubs.acs.org/JPCC

Effects of Protic and Aprotic Solvents in Mesoporous Silica: Tuning the UV−Vis Emission Properties by Means of Surface Activation

Carlo M. Carbonaro,* Riccardo Corpino, Pier Carlo Ricci, Daniele Chiriu, and Marcello Salis

Department of Physics, University of Cagliari, Campus of Monserrato, s.p. no. 8, km 0.700, 09042 Monserrato, Italy

Supporting Information

ABSTRACT: The emission properties of mesoporous silica in the visible and ultraviolet range are affected by the reaction of the surface centers with different nonpolar and protic/aprotic polar solvents, that is, oxidized water, acetone, chloroform, and methanol. The samples were analyzed under wet conditions and after annealing above 60 °C, showing that the quantum efficiency of the emission is strongly reduced by the presence of residual solvent engulfed within the pores of the samples. The relative weight of the two main emission bands recorded at about 320 and 400 nm depends on the solvent, the contribution of the UV band being larger in the case of methanol treatment. The recorded changes in the emission spectrum are compared with the ones detected in samples with different pore diameters treated with oxidized water and annealed at 90 °C. The reported data are interpreted within the scenario of the emitting surface centers, and their models are discussed in view of the effects of the reaction with different solvents and the porosity of the samples: the reaction to oxygen pressure of methanol-treated samples is discussed in terms of adsorption and desorption from the emitting centers.

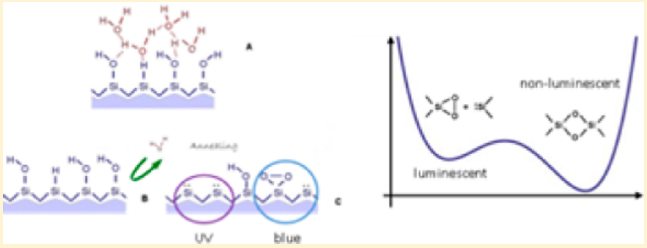

INTRODUCTION

Nanosized materials display novel physical, chemical, and optical properties related to the large surface to volume ratio and to quantum confinement effects, which can be exploited in nanoscale devices for electronics, optics, and bioengineering.[1−8] Among the others, nanostructured silica finds a number of applications because of its dielectrics properties and biocompatibility, ranging from electronic nanoarchitetures to nanophotonics and nanomedecine.[9] The incorporation of organic molecules within porous silica or silica nanoparticles allows preparing organic−inorganic hybrids for very efficient probing of biological tissue,[10] the probe being also responsive to magnetic field in the case of bimodal doping.[11] Besides the mass of silica-based hybrids, nondoped amorphous silica-based materials also exhibit two quite efficient broad photoluminescence (PL) bands in the UV−blue regions of the light spectrum (at 300−350 and 400−450 nm, respectively),[12,13] whose high emission quantum yield (about 20−30% depending on the synthesis conditions[13]) boosted the research to exploit nanosized silica as a light emitter integrated in Si-based nanoelectronics or as a probe of the structural properties of the insulating layer.[14−16] The two bands are characterized by non-single-exponential nanosecond decays and excitations in the UV (at 200 and 230 nm for the UV band and at 250 and 350 nm for the blue one). Due to the large surface area and the effects caused by different physical and chemical treatments, such as thermal annealing, vacuum or gas purging, interaction with polar or nonpolar solvents or acids,[17−24] it is generally believed that the PL recorded in nanostructured silica arises from some defect-related mechanisms. The nature and origin of the PL centers are still debated, and different hypotheses have been proposed to account for the reactivity of the silica surface and the possible contribution of different chemical species bonded to the silica surface.[23−26] For example, surface defects such as carbon impurities,[27] oxygen-related defects,[25,26,28] or photoinduced donor−acceptor pairs of nitrogen-related species[29] have been discussed so far. The presence of siloxane and silanol groups at the surface layer and within the nanometric silica skeleton play a key role in the structural and optical features of nanosized silica, modifying the structural properties of the silica matrix with respect to the bulk silica[30] and promoting the interaction with the surrounding environment.[17,28] Silanol species, in particular, are regarded as the starting ingredients to produce the emitting species in the UV and blue range, two different dehydroxylation mechanisms being proposed as the leading processes to induce those emissions: due to heating and/or vacuum treatments, two geminal silanols react to produce two distinct surface defect pairs, two facing silylene defects for the UV band and a silylene plus a dioxasilirane pair for the blue one.[18,21,25] However, despite the soundness of the proposed models versus experimental data and simulations for the blue band, for the UV one the harder excitation channels and its dependence on the synthesis conditions largely prevented systematic studies in the literature. Indeed, the UV band is the main PL in aerogel samples produced by condensation of alkoxysilane in H_2O−

Received: September 2, 2014
Revised: October 17, 2014
Published: October 17, 2014

   dx.doi.org/10.1021/jp508857t | J. Phys. Chem. C 2014, 118, 26219−26226

alcohol solution, with no need of reduction,[25] and its modifications under different conditions have been scarcely investigated. In addition, recent results on irradiation induced effects questioned the attribution of the blue band.[31] Intriguingly, if the two centers share a common origin, it should be possible to modify the relative contribution of the two bands by chemical or physical treatments: by removing an oxygen molecule from the blue center, we should get an UV one, or, on the contrary, by increasing the content of disposable molecular oxygen at the silica surface, we should convert UV centers into blue ones.

In recent years our endeavor has been dedicated to the characterization of the optical features of mesoporous silica, an ideal benchmark of nanostructured silica with a very large specific surface area, up to 600 m^2/g in the investigated samples, and skeleton walls in the nanometer range. The emission properties in the UV and blue range have been investigated as a function of the pore diameter, that is, the hydrophilic character of the silica surface,[32] and as a function of different environment conditions, that is, by analyzing the effects of long air exposure,[33] vacuum treatment,[26] oxygen or nitrogen purging, and interaction with strongly oxidizing polar solvent (H_2O_2).[22,23] To get further detailed insight into the PL features of nanosized silica, in the present work we analyzed the emission properties under different conditions, that is, by probing the silica surface with different protic or aprotic solvents to induce modification on the emitting centers. The effects of strongly oxidizing conditions are also investigated in samples with different pore diameters. Finally, the kinetics of the surface reactivity was also studied by monitoring the emission properties under sequence of vacuum and oxygen atmosphere. The reported results are discussed within the framework of the proposed dehydroxylation models. Besides providing further experimental tests to ascertain the origin of the emitting defects, our results clearly indicate the possibility to change the distribution of the emitting centers by properly activating the surface, in particular with methanol, to obtain an efficient and promising emission in the UV range. The challenging idea is that the interaction with polar solvents and oxygen gas can modify the spectral properties of the mesoporous silica surface emissions allowing tuning of the emission itself.

EXPERIMENTAL SECTION

Materials. The investigated samples are sol−gel synthesized commercial porous silica monoliths (diameter, 5 mm; thickness, 2 mm) produced by Geltech Inc. (USA) with pore diameter distribution sharply peaked at 3.2, 7.5, and 18.2 nm (BET analysis, 5% of standard deviation). In the following the three sets of samples are identified as A (pore diameter, 3.2 nm), B (pore diameter, 7.5 nm), and C (pore diameter, 18.2 nm), as reported in Table 1 with the sample porosity features.

Table 1. Porosity Features of Mesoporous Silica Samples

sample ID	pore diameter (nm)	SSA[a] (m^2/g)	pore volume (cm^3/g)	mass density (g/cm^3)
A	3.2	594	0.488	1.2
B	7.5	525	1.000	0.7
C	18.2	264	1.203	0.6

[a]SSA, specific surface area.

Due to possible contamination because of air exposure, all of the samples were subjected to a preconditioning bleaching procedure with oxidized water (30% vol). The samples were filled with H_2O_2 and thermally treated at 90 °C to remove possible contamination, as reported in a previous work.[33] After preconditioning, the samples were annealed at 90 °C to remove the water nested within the pores and then soaked with different solvents, acetone, chloroform, or methanol. All of the solvents were of spectroscopic grade. Finally, the samples were annealed at 65 °C to remove the residual solvent from the pores. The whole set of samples was analyzed under wet conditions and after thermal annealing at 90 °C for the H_2O_2 case and at 65 °C for the other solvents.

In the figures, the different solvents are indicated as AC (acetone), CHL (chloroform), MET (methanol), and W (oxidized water). T indicates annealed samples.

Methods. Time-resolved PL (TR-PL) was carried out by exciting the sample with the emission at 250 nm of an optical parametric oscillator with frequency doubler device (Spectra Physics MOPO), seeded by a pulsed Nd:YAG laser (Spectra Physics QuantaRay PRO-270). The excitation pulse energy was about 1 mJ/pulse, and the pulse width at half-maximum was 6 ns with a 10 Hz repetition rate. PL measurements were performed in 90° geometry, focusing the emitted light signal onto the entrance slit of a monochromator (ARC Spectra Pro 300i) with a spectral bandwidth of 12 nm. The signal was detected by a gatable intensified CCD (Princeton Instruments PIMAX). Depending on the PL bands under examination, different time delays from excitation pulse and time gates were used. The reported PL spectra were recorded by applying a short wavelength cutoff filter (WG280) and corrected for the optical transfer function of the system.

Raman scattering measurements were performed with a Raman spectrometer (Dilor XY800). An argon ion laser operating at 514.5 nm (Coherent Innova 90C-4) supplied the excitation. The signal, dispersed with 600 grooves/mm grating, was detected by a 1024 × 256 liquid N_2 cooled charge coupled detector (CCD). All Raman scattering measurements were performed with a spectral resolution of about 2 cm^{-1}, at room temperature.

The sensitivity of the samples to the O_2 pressure of the surrounding environments was tested by measuring the PL spectrum under different oxygen exposure/vacuum cycles: starting with the samples in equilibrium with air, the sample chamber was evacuated to 10^{-2} Torr and successively filled with O_2 (equilibrium pressure of 2×10^3 Torr). The procedure was repeated a few times, and then the sample chamber was restored to pristine conditions (air).

RESULTS

The whole set of samples was subjected to a bleaching procedure with hydrogen peroxide, which allows the removal of the possible presence of pollutants on the silica surface and testing of the surface reactivity to oxidized water as a function of sample porosity. As already reported in previous papers,[22,33] the treatment with oxidized water recovers the pristine transparency of the samples and removes the contaminants adsorbed at the silica surface from the environments. Figure 1 reports the emission properties recorded in the samples after the bleaching procedure, before and after annealing at 90 °C (Figure 1, panels a and b, respectively), excited at 250 nm. The reported spectra were recorded at zero time delay from the excitation light with a gate window of 100 ns to collect the

dx.doi.org/10.1021/jp508857t | J. Phys. Chem. C 2014, 118, 26219−26226

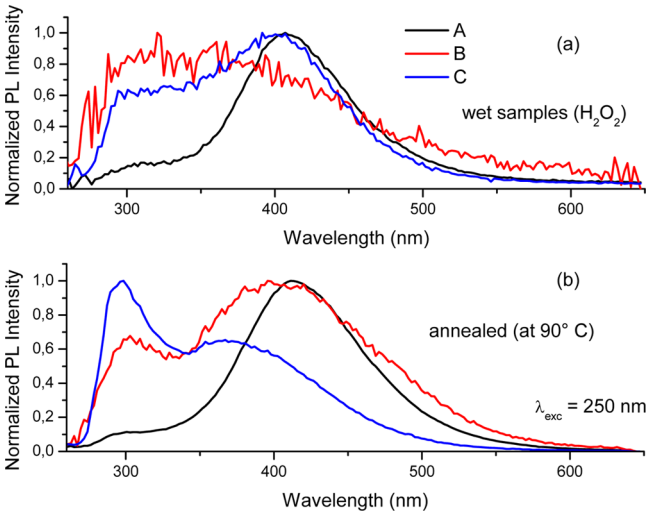

Figure 1. Emission properties after bleaching procedure, before (a) and after (b) annealing at 90 °C, excited at 250 nm.

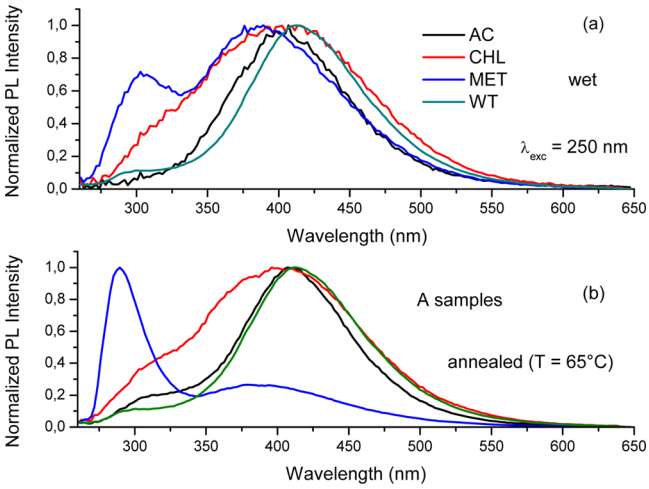

Figure 2. PL spectra of A samples soaked with acetone, chloroform, and methanol compared to preconditioned samples, before (a) and after (b) annealing at 65 °C (excited at 250 nm).

overall emission of the samples. The spectra were arbitrarily normalized to unity for shape comparison.

Two main contributions are shown, their relative weight depending on the sample porosity: a band at about 410 nm (in the following, the blue band) and a band peaked at about 320 nm (hereafter the UV band). The relative ratio of the two bands depends on the porosity of the investigated samples, the contribution of the UV band being in general larger in samples with larger pore diameter. The trend is better observed after annealing of the samples at 90 °C, as depicted in Figure 1b: the relative contribution of the UV band with respect to the blue one increases as the sample pore diameter increases. In addition, the peak position of the blue band undergoes a blue shift from 400 nm in A samples to 380 nm in C samples. The overall emission spectrum largely increases after annealing in the whole set of samples, the recorded emission being 5−10 times larger than in wet conditions.[34] However, it is pointed out that the shape of the spectrum is not modified by the annealing procedure (see S1 in the Supporting Information). S2 reports the non-single-exponential decay time of the recorded emissions for the A samples: the plots were fitted with two exponential decays of about 4 and 20 ns in both cases (see Table II for details). Under wet conditions, however, the decay time of the UV band in B and C samples was single exponential, the fast component at about 3 ns being the only band detected in this case, whereas the time features of the blue band were almost identical. We have to emphasize that the fast decays are at the limit of the sensitivity of our detection system and the relative UV contribution is small compared to the blue one. In addition, with regard to the emission efficiency, within the assumption of comparable experimental conditions in terms of excitation power and signal collection, we can qualitatively estimate that A samples are 10 times more efficient than B and C samples.

The effects of protic and aprotic solvents were investigated in dried A samples. By soaking the samples with different solvents, the overall emission efficiency decreases and the spectral features of the samples are modified. Figure 2a reports the normalized PL spectra of samples soaked with acetone, chloroform, and methanol as compared to the PL spectrum of the bleached samples after the treatment with oxidized water and the subsequent annealing. In the presence of acetone, the blue emission slightly blue shifts (from 413 to 402 nm), whereas the contribution of the UV band is barely detectable. In the case of chloroform, the spectral width of the blue band largely increases and the UV band is now recorded as a shoulder of the blue one. Finally, when the samples are rinsed with methanol, the two bands are spectrally well resolved, the blue band being shifted at about 390 nm and increased in its bandwidth, whereas the relative contribution of the UV band, detected at about 305 nm, is about two-thirds in intensity of the contribution of the blue band. To summarize, one can observe that the relative UV weight with respect to the blue one increases following the trend from acetone to H_2O_2 (almost identical), then to chloroform, and finally to methanol.

The annealing at 65 °C increases the quantum yield of the overall emission spectrum regardless of the solvent treatment investigated (Figure 2b). The increased emission efficiency was estimated by calculating the ratio between the integral area of the PL curve under wet conditions and after annealing: the recorded increase was 19 times that in the acetone case, about 5 times that for the chloroform, and about 8 times that in the case of methanol. However, the annealing affects in different ways the spectral shape of the emission spectrum, modifying the spectral position or the relative contribution of the detected bands. Indeed, the UV relative weight with respect to the blue one still depends on the solvent following a comparable trend (H_2O_2, acetone, chloroform, and methanol), but a large spectral modification is recorded in the methanol case, the UV band being the highest one with a contribution about 3 times higher than the blue one.

Decay features recorded after treatment with different solvents are similar to the ones gathered in the H_2O_2 case; after annealing, two exponential decays of about 3−5 and >10 ns were applied to successfully fit the emission decay at 402 nm in both wet and annealed conditions, whereas the decay of the 320 nm band was in general single-exponential under wet conditions and non-single-exponential after annealing (see Table II in the Supporting Information for details).

The Raman spectra recorded after annealing are reported for the acetone and methanol case (Figure 3a). The typical vibrational bands of silica are detected, with very small contributions of the so-called D_2 and ω_3 bands. The silanol vibration at 980 cm^{-1} is also recorded in both samples. No

dx.doi.org/10.1021/jp508857t | J. Phys. Chem. C 2014, 118, 26219−26226

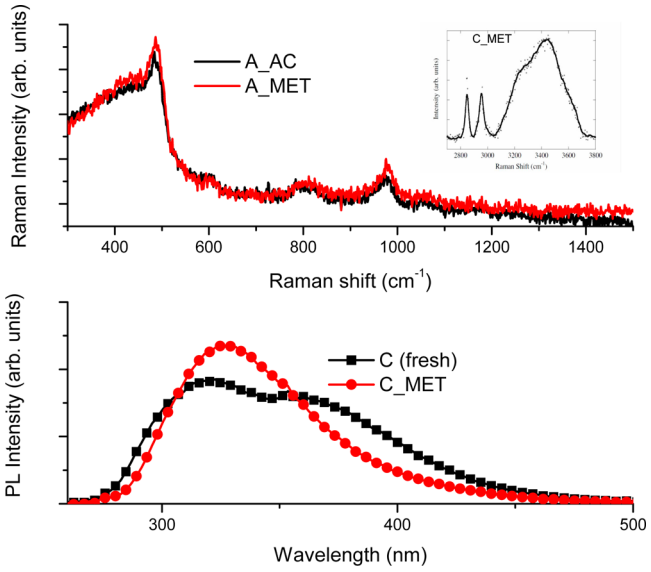

Figure 3. (a, top) Raman spectra of annealed A samples after acetone and methanol treatment; inset shows the Raman spectrum in the 2600−3800 cm^{-1} range for the C samples after methanol treatment. (b, bottom) PL spectra of fresh and annealed C samples after methanol treatment.

solvent-related bands were recorded, neither in the higher cm^{-1} range, here not reported because of the very poor signal-to-noise ratio. In the case of wet samples, for example, A and C samples treated with methanol, the presence of the latter can be retrieved by means of the vibration at about 1030 cm^{-1} (see S3 in the Supporting Information).

The inset shows the higher cm^{-1} range for the case of C samples after methanol treatment (rinsing and annealing at 65 °C). The procedure was performed on fresh samples, so that the H_2O_2 preconditioning bleaching procedure was not performed, because the samples were optically transparent, free of pollutants: in this case one can observe a large contribution in the 3000−3400 cm^{-1}, due to the presence of engulfed water and interacting surface silanols, and two sharp bands at 2846 and 2956 cm^{-1} related to residual methanol and assigned to the C−H symmetric and antisymmetric stretching, respectively. These findings are a clear indication that in the case of C samples a longer annealing is required; once performed, no signal of residual solvents is recorded.

The emission spectrum of methanol-treated C sample recorded under 250 nm excitation is reported in Figure 3b together with the PL spectrum of the fresh sample for comparison. The latter shows the same spectral feature reported in Figure 1b for preconditioned samples with the presence of the two bands at about 380 and 320 nm, the UV contribution being the largest. After methanol treatment, the contribution of the blue band is largely reduced, being a shoulder of the main UV band. The decay time of the 320 nm emission is comparable with the data reported for A samples (see the Supporting Information for details).

With regard to the relative emission efficiency, one can observe that before annealing, the PL efficiency increases from acetone to chloroform and finally to methanol; after annealing, acetone and chloroform switched their positions, the PL efficiency in the methanol case still being the largest.

In Figure 4 the PL intensity of the blue and UV peaks in the A samples after methanol treatment is reported as a function of

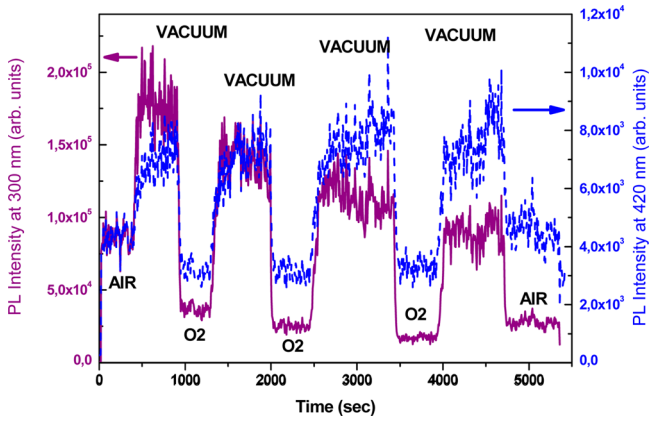

Figure 4. PL intensity of the blue and UV peaks in A samples after methanol treatment as a function of time (repeated cycles of evacuation and O_2 pressurization, see text for details).

time while the O_2 pressure in the sample chamber is changed. The blue emission (Figure 4) is increased when the vacuum is performed in the sample chamber, and it is decreased when the sample chamber is filled with oxygen. In both cases a saturation trend is observed, the final PL intensity reached in each step being constant within the experiment observation time. Finally, the sample chamber is reported to atmospheric conditions, and the PL intensity at 400 nm recovers the pristine value. The trend recorded for the UV band (Figure 4) shows important differences: whereas the general trend is similar, the PL intensity being increased under vacuum conditions and decreased under oxygen pressure, the PL intensity undergoes a decrease during vacuum time observation, as for the oxygen case, and the final PL intensity reached in both situations is smaller than the previous one. Indeed, the PL intensity recorded at the end of the experiment, once the sample is reported to atmospheric conditions, is smaller than the value recorded at the starter, the final value being about 50% of the starting one. A similar consideration applies for the final value under vacuum conditions as compared to the starting value under the same conditions.

DISCUSSION

Nanosized silica presents a variety of emissions in the UV−visible spectral range, which are typically related to or affected by the large surface area and the nanoscale dimensions.[13] Among the different centers, our ongoing endeavor has been dedicated to the analysis of the UV and blue bands recorded in the 300−450 nm range, a spectral region of interest for photonic applications in silica−silicon integrated devices and lightening technology. The studies reported in the literature in the past decades on different kinds of nanodimensioned silica, in particular concerning the blue emission, which is also reported for oxidized nanostructured silicon,[35,36] allow us to establish a few key points: (i) the emission bands are related to O_2-derived surface defects;[13,28] (ii) the presence of surface silianol species is required to produce or enhance the emission efficiency but cannot be considered as the emitting center themselves because of the hard excitation of the SiOH groups (above 7.5 eV);[13,17] (iii) the contribution of possible C-related pollutants collected at the surface from the surrounding environments or as residual of the synthesis procedure is not responsible for the UV band,[22] neither of the blue one, but for a small contribution that can be recognized by its decay time

dx.doi.org/10.1021/jp508857t | J. Phys. Chem. C 2014, 118, 26219−26226

(above 60 ns);[33,37] (iv) in the case of mesoporous silica, the porosity of the samples determines the hydrophilic character of the surface and affects the distribution of the emitting centers;[32,33] (v) comparable surface defects have been reported for a variety of nanosized oxides, such as ZnO, MgO, and Al_2O_3, suggesting a possible common origin of the centers.[13] The sensitivity to the surrounding environment was largely exploited to investigate the nanostructured silica emissions to understand the chemical and physical composition of the defects. It was reported, for example, that the interaction with mineral acids can augment the efficiency of trapping processes in silica nanostructures, most possibly through the protonation of trap states and causing a change in the color of the PL from blue to bluish green.[24] A slight red shift of the blue band, coupled with a large quenching of its intensity, was also shown by adding H_2O_2 to silica nanoparticle suspensions.[17] In addition, time-resolved PL measurements evidenced an increase of the longer decay time of the biexponential decay of the blue band in polar media and even more in protic media.[17] Within the framework of the silylene-based models proposed by Uchino, the short component of the biexponential blue PL decay has been attributed to the germane emission center and the long one to surface trap states. The blue PL long component depends on the surface morphology, and it was inferred that the interaction with the solvent molecules in polar media stabilizes the surface trap states especially by hydrogen bonding with alcohols.[17] Also, the UV band displays a biexponential decay, and a similar interpretation can be assumed because of the hypothesized common origin of the band (dehydroxylation mechanism under vacuum conditions). Besides the quantum mechanical calculations,[18,21,25] the formation of silylene, dioxisilirane, and edge-shared silicon thetrahedra (see later) was reported in a number of close molecular systems,[39,40] the optical properties being quite in agreement with ones here reported.

In the present paper we were driven by the challenging idea that if the dehydroxylation models previously proposed to explain the UV and blue bands are correct, the interaction with polar solvents and oxygen gas should modify the spectral properties of the two emissions and change their relative contribution to the overall spectrum. In particular, because the UV center is a sort of O_2-deprived blue center, the intriguing idea was to find the way to tune the emission of mesoporous silica by proper interaction with the surrounding environment. To achieve this ambitious target and, at the same time, to shed light on the attribution of the two bands, we carried out different treatments of the silica surface of mesoporous samples exploiting the sensitivity of the emission features to the surrounding environments as a probe of the surface centers themselves.

The preconditioning procedure allows us not only to restore the pristine transparency of the samples, as already reported,[22,33] but also to discuss the effects of the presence of water within samples with different pore diameters (wet conditions) and to compare them with the annealed conditions in terms of luminescence features. The effectiveness of the preconditioning procedure can be easily evaluated considering the emission properties of the recorded PL bands, which agree well with the ones of fresh samples but for small shifts of the peak positions and relative intensity, as also inferred by comparing PL spectra of preconditioned and fresh C samples (Figures 1b and 3b, respectively). The procedure evidences two main aspects: the quenching effect of the solvent and the relationship of the relative ratio of the two PL bands with the sample porosity. The reduced emission efficiency of the centers under wet conditions can be ascribed to the formation of a cage-like structure of the solvent covering the pore walls and chemically or physically interacting with the emitting centers, at least by means of steric hindrance. The interaction allows the formation of new and/or more efficient nonradiative de-excitation pathways, which decrease the quantum yield of the emissions.

On the basis of the increase of the long tail of time decay of the blue emission,[17] it was reported that hydrogen peroxide can react with a defect pair, leading to the formation of nonluminescent center and stabilizing surface states. In the present samples, as reported in Table II, under wet conditions the recorded decays were single exponential but for the A samples, for which two lifetimes of about 6 and 30 ns were detected. However, in the case of samples with larger pore diameters (B and C), a constant background was added to successfully fit the data with single-exponential decays, a background that could be the effect of a very long emission whose contribution in the nanosecond time domain is very small.

The second aspect the preconditioning procedure discloses is the dependence of the relative weight of the two main emission bands on the sample porosity, showing a larger contribution of the UV band in samples with larger pore diameters. This relationship can be interpreted within the framework of the silanol-related model proposed for the two emitting centers and schematically pictured in Figure 5a. Indeed, it was previously reported that the hydrophilic character of mesoporous silica

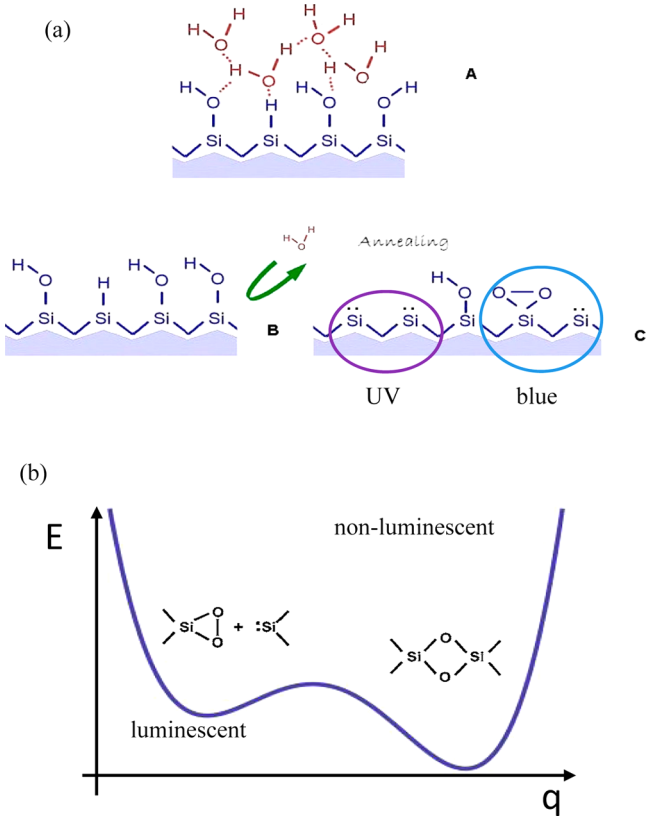

Figure 5. (a) Scheme of formation of UV and blue centers at silica surface. (b) Scheme of energy versus configuration coordinate for blue center.

dx.doi.org/10.1021/jp508857t | J. Phys. Chem. C 2014, 118, 26219−26226

samples depends on their porosity, samples with larger pore diameter being more hydrophilic than samples with smaller pore diameter.[32] The dependence on the pore diameter is better evidenced in annealed samples, where the relative contribution of the UV band increases as the pore diameter increases. Simulations previously carried out on the silianol-related models of the two bands reported that the distance between Si atoms in the UV center is larger than in the blue one.[18,21,25] In addition, the same works showed that the blue defect is metastable, and as the distance between adjacent Si atoms increases, it can relax in the nonemitting edge-sharing tetrahedra defect, as depicted in Figure 5b.[21,38] This is in good agreement with the observed data, the crucial parameter being the curvature of the silica surface: as the curvature decreases, the distance between silanols increases, favoring the formation of UV centers against blue ones.

The wetting effect was also confirmed with different solvents, showing a dependence on the polarity of the solvent: indeed, the quenching ratio was the largest for hydrogen peroxide and acetone, the ones with largest dipole moment, and smaller for chloroform and methanol, suggesting the role of the electrostatic interaction between the solvent and the surface emitting centers.

It was previously reported for silica nanoparticles that the interaction with solvent, and in particular with protic ones, produces the stabilization of surface traps via hydrogen bonding, leading to a larger contribution of the long component in the blue PL decay curves.[17] With reference to the details of the decays' analysis reported in Table II of the Supporting Information, it is interesting to note that in the present study we did not observe very large differences on the relative contribution of the longer component of the blue band under wet and annealed conditions for all of the solvents but for the acetone case, where a large increase was recorded. The same trend is also true for the UV emission, but we have to mention that in general under wet conditions the signal-to-noise ratio of the UV contribution was poorer and the decay was single-exponential. This is an indication, in our opinion, that the interaction of the solvents with the emitting centers affects in the same way both the short and long components, suggesting a physical interaction, like steric hindrance, instead of a chemical bonding, the interaction being able to suppress the longer contribution in the UV case. However, a detailed analysis with an ultrafast facility is mandatory, in particular to better ascertain the contribution of the shortest component, which is at the limit of our system resolution.

The most striking result after annealing is the large increase of the UV band in methanol-treated samples, which can be rationalized by hypothesizing that the blue centers can react with methanol, producing carbon dioxide and water and transforming the blue centers in the UV ones, so leading to the reported relative increase of the latter. This is an extra proof that the proposed silanol-related models for the UV and blue centers are quite sound and pinpoint the possibility to modify the distribution of the emitting centers by proper interaction with selected solvents, in particular methanol. The further step is to verify the reversibility of the process, namely, the possibility to convert UV centers in blue ones by interaction with oxygen molecules and to analyze the kinetics of the interaction of the emitting centers with oxygen. The effects of successive cycles of evacuation and oxygen pressurization were monitored by plotting the intensity of the UV and blue emissions as a function of time in A samples previously treated with methanol, namely, with a larger contribution of the UV band. The kinetics curves indicate that the adsorption and desorption of oxygen affect the emissions of both centers, leading to a decrease of the overall emission during adsorption and an increase during desorption. However, there are important differences: whereas the starting intensity of the blue PL recorded in air before the vacuum/O_2 cycles started was recovered at the end of the treatment, the one of the UV band was decreased by 50%, showing a permanent modification of about half of the emitting centers. In addition, after the initial increase, during vacuum iterations the UV PL undergoes a decrease, whereas the blue band displays a saturation trend. The overall increase of the emission spectrum and the saturation trend of the blue band under evacuation can be related to the removal of oxygen molecules from the surface whose presence has a detrimental effects on the emission efficiency, probably due to steric hindrance. How can we explain the decrease of UV band during evacuation? We have already shown in a previous paper that oxygen purging can indeed modify the relative contribution of the two bands, leading to a decrease of the UV one.[23] Without entering into the details of the kinetics, which will be discussed in a further work, the reported decrease of the UV band can be interpreted as the transformation of UV centers into nonemitting centers. Indeed, at the end of the cycles the number of UV emitting centers, namely, the intensity of the UV band, is decreased to 50% of the starting value. This effect recalls the previously reported transition of the blue center into a nonemitting edge-sharing tetrahedra defect: if we assume that also the UV center is in a metastable configuration, then its transition into a nonemitting configuration could be promoted by the interaction with the excitation light. It is worth noting that the UV center is a sort of oxygen vacancy, which was reported to be responsible of the absorption at 7.6 eV in bulk silica and to have a metastable character related to two different configurations, called puckered (distorted) and unpuckered (fully relaxed).[41] If bulk silica is irradiated with, for example, γ irradiation, the well-known nonemitting E′ center is formed. The E′ center is a positively charged oxygen vacancy in the puckered configuration. We can speculate that at the silica surface a large number of distorted centers are present, so the decrease of the UV band could be obtained with the following mechanism: upon light excitation, the electron of the UV center is captured by one of the numerous surface traps; thus, the center could be transformed into an E′ center. Indeed, irradiation by γ rays of mesoporous silica caused the decrease of the relative contribution of the UV band and the formation of E′ centers.[42] Although intriguing and sound, further experimental proofs are needed to verify this hypothesis.

CONCLUSIONS

The UV and visible emissions of mesoporous silica in the 300−450 nm are largely affected by the interaction with different nonpolar and protic/aprotic polar solvents, due to the reaction of the emitting surface centers with the surrounding environment. Under wet conditions the overall emission spectrum is largely reduced due to a cage-like effect that promotes nonradiative de-excitation pathways. Once annealed at proper evaporation temperature, the overall emission increases with no changes in the spectral shape. The analysis of samples with different porosities soaked with the same solvent (namely, H_2O_2) and the ones at fixed porosity with different solvents enlightens the possibility to tune the emission spectrum by

increasing the porosity or by modifying the distribution of the emitting center because of the reactions induced by the presence of methanol: in both cases the relative contribution of the UV band is increased with respect to that of the blue band. The induced modifications are not reversible, as shown by oxygen/evacuation cycles, and a possible correlation with the formation of nonluminescent E′ centers is suggested to explain the not reversible decrease of the UV contribution during the oxygen/evacuation cycles.

■ ASSOCIATED CONTENT

Supporting Information

Comparison of wet and annealed PL spectra (S1), time decay curves (S2), and their fitting results (Table II). This material is available free of charge via the Internet at http://pubs.acs.org.

■ AUTHOR INFORMATION

Corresponding Author

*(C.M.C.) E-mail: cm.carbonaro@dsf.unica.it. Phone: 0039 070 6754823. Fax: 0039 070 6753191.

Author Contributions

The manuscript was written through contributions of all authors. All authors have given approval to the final version of the manuscript.

Notes

The authors declare no competing financial interest.

■ ABBREVIATIONS

AC, acetone; CHL, chloroform; MET, methanol; W, oxidized water; PL, photoluminescence; TR-PL, time-resolved PL

■ REFERENCES

(1) Morale, A. M.; Lieber, C. M. A Laser Ablation Method for the Synthesis of Crystalline Semiconductor Nanowires. *Science* **1998**, *279*, 208−211.

(2) Duan, X.; Lieber, C. M. General Synthesis of Compound Semiconductor Nanowires. *Adv. Mater.* **2000**, *12*, 298−302.

(3) Fan, S.; Chapline, M. G.; Franklin, N. R.; Tombler, T. W.; Cassell, A. M.; Dai, H. Self-Oriented Regular Arrays of Carbon Nanotubes and Their Field Emission Properties. *Science* **1999**, *283*, 512−514.

(4) Bonacchi, S.; Genovese, D.; Juris, R.; Montalti, M.; Prodi, L.; Rampazzo, E.; Zaccheroni, N. Luminescent Silica Nanoparticles: Extending the Frontiers of Brightness. *Angew. Chem., Int. Ed.* **2011**, *50*, 4056−4066.

(5) Tripathi, N.; Yamashita, M.; Akai, T. Synthesis and Improved Emission Characteristics of BCNO@silica Composites. *J. Mater. Chem. C* **2014**, *2*, 622−625.

(6) Gandhi, S.; Thandavan, K.; Kwon, B.-J.; Woo, H.-J.; Kim, C. H.; Yi, S.; Jeong, J. H.; Shinf, D.-S.; Jang, K. A Highly Efficient Warm White Light-emitting Eu^{2+}-activated Silicate Host: Another Striking Application of Mesoporous Silica. *J. Mater. Chem. C* **2014**, *2*, 6630−6636.

(7) Tao, S.; Fan, P.; Wang, Y.; Wang, C.; Hu, T.; Meng, C. Multifunctional Fluorescent Material Based on Metallomicelles Trapped in Silica Nanochannels. *J. Mater. Chem. C* **2014**, *2*, 1962−1965.

(8) Ricci, P. C.; Casula, R.; Gulleri, G.; Fumagalli, F.; Carbonaro, C. M.; Corpino, R. Mechanical Stress in Silicon Nanosized Architectures: Defects of SOD Processed Silica Filler. *J. Alloys Compd.* **2014**, *602*, 157−162.

(9) Cui, Y.; Zheng, X.-S.; Ren, B.; Wang, R.; Zhang, J.; Xia, N.-S.; Tian, Z.-Q. Au@organosilica Multifunctional Nanoparticles for the Multimodal Imaging. *Chem. Sci.* **2011**, *2*, 1463−1469.

(10) Cho, E.-B.; Volkov, D. O.; Sokolov, I. Ultrabright Fluorescent Mesoporous Silica Nanoparticles. *Small* **2010**, *6*, 2314−2319.

(11) Yang, P.; Gai, S.; Lin, J. Functionalized Mesoporous Silica Materials for Controlled Drug Delivery. *Chem. Soc. Rev.* **2012**, *41*, 3679−3698.

(12) Anedda, A.; Carbonaro, C. M.; Clemente, F.; Corpino, R.; Ricci, P. C. Time Resolved Ultraviolet Photoluminescence of Mesoporous Silica. *J. Phys. Chem. B* **2005**, *109*, 1239−1242.

(13) Anjiki, A.; Uchino, T. Visible Photoluminescence from Photoinduced Molecular Species in Nanometer-Sized Oxides: Crystalline Al_2O_3 and Amorphous SiO_2 Nanoparticles. *J. Phys. Chem. C* **2012**, *116*, 15747−15755.

(14) Tong, L. M.; Gattass, R. R.; Ashcom, J. B.; He, S. L.; Lou, J. Y.; Shen, M. Y.; Maxell, I.; Mazur, E. Subwavelength-diameter Silica Wires for Low-loss Optical Wave Guiding. *Nature* **2003**, *26*, 816−819.

(15) Tong, L.; Lou, J.; Gattass, R. R.; He, S.; Chen, X.; Liu, L.; Mazur, E. Assembly of Silica Nanowires on Silica Aerogels for Microphotonic Devices. *Nano Lett.* **2005**, *5*, 259−262.

(16) Ricci, P. C.; Gulleri, G.; Fumagalli, F.; Carbonaro, C. M.; Corpino, R. Optical Characterization of Polysilazane Based Silica Thin Films on Silicon Substrates. *Appl. Surf. Sci.* **2013**, *265*, 470−474.

(17) Banerjee, S.; Honkote, S.; Datta, A. Interaction of Surface Trap States and Defect Pair of Photoluminescent Silica Nanostructures with H_2O_2 and Solvents. *J. Phys. Chem. C* **2011**, *115*, 1576−1581.

(18) Uchino, T.; Kurumoto, N.; Sagawa, N. Structure and Formation Mechanism of Blue-light-emitting Centers in Silicon and Silica-based Nanostructured Materials. *Phys. Rev. B* **2006**, *73*, No. 233203.

(19) Banerjee, S.; Datta, A. Photoluminescent Silica Nanotubes and Nanodisks Prepared by the Reverse Micelle Sol-Gel Method. *Langmuir* **2010**, *26*, 1172−1176.

(20) Shang, N. G.; Vetter, U.; Gerhards, I.; Hofsass, H.; Ronning, C.; Seibt, M. Luminescence Centres in Silica Nanowires. *Nanotechnology* **2006**, *17*, 3215−3218.

(21) Sagawa, N.; Uchino, T. Effect of Annealing on the Visible Photoluminescence Characteristics of Octadecyltrichlorosilane Monolayers on Silica Surfaces. *J. Phys. Chem. C* **2008**, *112*, 4581−4589.

(22) Carbonaro, C. M.; Corpino, R.; Ricci, P. C.; Salis, M.; Anedda, A. Changing the Environment of Mesoporous Silica to Investigate the Origin of UV and Visible Photoluminescence of Surface Centers. *J. Mater. Sci.* **2013**, *48*, 4452−4458.

(23) Carbonaro, C. M.; Corpino, R.; Ricci, P. C.; Chiriu, D. Sensitivity to Oxygen Environments of Mesoporous Silica Samples With Different Porosities. *J. Non-Cryst. Solids* **2014**, *401*, 60−65.

(24) Banerjee, S.; Maity, S.; Datta, A. Enhanced Trapping Efficiency in Acid-Treated Silica Nanostructures. *J. Phys. Chem. C* **2011**, *115*, 22804−22809.

(25) Aboshi, A.; Kurumoto, N.; Yamada, T.; Uchino, T. Influence of Thermal Treatments on the Photoluminescence Characteristics of Nanometer-Sized Amorphous Silica Particles. *J. Phys. Chem. C* **2007**, *111*, 8483−8488.

(26) Carbonaro, C. M.; Chiriu, D.; Corpino, R.; Ricci, P. C.; Anedda, A. Photoluminescence Characterization of Sol−Gel Prepared Low Density Silica Samples. *J. Non-Cryst. Solids* **2007**, *353*, 550−554.

(27) Green, W. H.; Le, K. P.; Grey, J.; Au, T. T.; Sailor, M. J. White Phosphors from a Silicate-Carboxylate Sol-Gel Precursor That Lack Metal Activator Ions. *Science* **1997**, *276*, 1826−1828.

(28) Nishimura, A.; Sagawa, N.; Uchino, T. Structural Origin of Visible Luminescence from Silica Based Organic−Inorganic Hybrid Materials. *J. Phys. Chem. C* **2009**, *113*, 4260−4262.

(29) Carlos, L. D.; de Zea Bermudez, V.; Amaral, S.; Nunes, S. C.; Silva, N. J. O.; Sá Ferreira, R. A.; Rocha, J.; Santilli, C. V.; Ostrovskii, D. Nanoscopic Photoluminescence Memory as a Fingerprint of Complexity in Self-Assembled Alkyl/Siloxane Hybrids. *Adv. Mater.* **2007**, *19*, 341−348.

(30) Alessi, A.; Agnello, S.; Buscarino, G.; Gelardi, F. M. Structural Properties of Core and Surface of Silica Nanoparticles Investigated by Raman Spectroscopy. *J. Raman Spectrosc.* **2013**, *44*, 810−816.

(31) Vaccaro, L.; Spallino, L.; Agnello, S.; Buscarino, G.; Cannas, M. Defect-related Visible Luminescence of Silica Nanoparticles. *Phys. Status Solidi C* **2013**, *10*, 658−661.
(32) Anedda, A.; Carbonaro, C. M.; Clemente, F.; Corda, L.; Corpino, R.; Ricci, P. C. Surface Hydroxyls in Porous Silica: a Raman Spectroscopy Study. *Mater. Sci. Eng. C* **2003**, *23*, 1069−1072.
(33) Carbonaro, C. M.; Ricci, P. C.; Corpino, R.; Marceddu, M.; Anedda, A. Photoluminescence Characterization of Aged and Regenerated Mesoporous Silica. *J. Non-Cryst. Solids* **2011**, *357*, 1904−1907.
(34) The increase of intensity is smaller than in ref 22 because the data were collected with a larger gate window to record also the contribution of the longer emissions.
(35) Ruckschloss, M.; Wirschem, T.; Tamura, H.; Ruhl, G.; Oswald, J.; Veprek, S. Photoluminescence from OH-related Radiative Centres in Silica, Metal Oxides and Oxidized Nanocrystalline and Porous Silicon. *J. Lumin.* **1995**, *63*, 279−287.
(36) Qin, G. G.; Lin, J.; Duan, J. Q.; Yao, G. Q. A Comparative Study of Ultraviolet Emission With Peak Wavelengths Around 350 nm from Oxidized Porous Silicon and That from SiO_2 Powder. *Appl. Phys. Lett.* **1996**, *69*, 1689−1691.
(37) Nishimura, A.; Harada, S.; Uchino, T. Effect of Cross-Linking and Organic Groups on the Visible Photoluminescence Characteristics of *n*-Octadecylsiloxanes. *J. Phys. Chem. C* **2010**, *114*, 8568−8574.
(38) Bunker, B. C.; Haaland, D. M.; Ward, K. J.; Michalske, T. A.; Smith, W. L.; Binkley, J. S.; Melius, C. F.; Balfe, C. A. Infrared Spectra of Edge-shared Silicate Tetrahedra. *Surf. Sci.* **1989**, *210*, 406−428.
(39) Patyk, A.; Sander, W.; Gauss, J.; Cremer, D. Difluoro- and Dichlorodioxasilirane. *Chem. Ber.* **1990**, *123*, 89−90.
(40) Bornemann, H.; Sander, W. Oxidation of Methyl(phenyl)-silylenesz: Synthesis of a Dioxasilirane. *J. Am. Chem. Soc.* **2000**, *122*, 6727−6734.
(41) Carbonaro, C. M.; Fiorentini, V.; Bernardini, F. Proof of the Thermodynamical Stability of the E′ Center in SiO_2. *Phys. Rev. Lett.* **2001**, *86*, 3064−3067.
(42) Anedda, A.; Carbonaro, C. M.; Corpino, R.; Agnello, S. Photoluminescent and Paramagnetic Centers in Gamma Irradiated Porous Silica. *J. Non-Cryst. Solids* **2005**, *351*, 1784−1786.